



Circulating HDL levels control hypothalamic astrogliosis via apoA-I^S

Anna Götz,^{*,†} Maarit Lehti,[§] Elizabeth Donelan,^{**} Cynthia Striese,^{††} Sebastian Cucuruz,^{††} Stephan Sachs,^{††} Chun-Xia Yi,^{§§} Stephen C. Woods,^{**} Samuel D. Wright,^{***} Timo D. Müller,^{*,†††} Matthias H. Tschöp,^{*,†††} Yuanqing Gao,^{1,§§§} and Susanna M. Hofmann^{1,†††,****}

Institutes for Diabetes and Obesity^{*} and Diabetes and Regeneration Research,^{††} Helmholtz Zentrum München, German Research Center for Environmental Health (GmbH), Neuherberg, Germany; Department of Internal Medicine I,[†] University Hospital RWTH Aachen, Aachen, Germany; LIKES Research Centre for Physical Activity and Health,[§] Jyväskylä, Finland; Metabolic Disease Institute,^{**} Department of Internal Medicine, University of Cincinnati, Cincinnati, OH; Department of Endocrinology and Metabolism,^{§§} Academic Medical Center, University of Amsterdam, Amsterdam, The Netherlands; CSL Behring,^{***} King of Prussia, PA; German Center for Diabetes Research (DZD),^{†††} München-Neuherberg, Germany; Nanjing Medical University,^{§§§} College of Pharmacy, Nanjing, China; and Medizinische Klinik und Poliklinik IV,^{****} Klinikum der Ludwig Maximilian Universität, Munich, Germany

Abstract Meta-inflammation of hypothalamic areas governing energy homeostasis has recently emerged as a process of potential pathophysiological relevance for the development of obesity and its metabolic sequelae. The current model suggests that diet-induced neuronal injury triggers microglia and astrogliosis, conditions which ultimately may induce functional impairment of hypothalamic circuits governing feeding behavior, systemic metabolism, and body weight. Epidemiological data indicate that low circulating HDL levels, besides conveying cardiovascular risk, also correlate strongly with obesity. We simulated that condition by using a genetic loss of function mouse model (apoA-I^{-/-}) with markedly reduced HDL levels to investigate whether HDL may directly modulate hypothalamic inflammation. Astrogliosis was significantly enhanced in the hypothalamus of apoA-I^{-/-} compared with apoA-I^{+/+} mice and was associated with compromised mitochondrial function. apoA-I^{-/-} mice exhibited key components of metabolic disease, like increased fat mass, fasting glucose levels, hepatic triglyceride content, and hepatic glucose output compared with apoA-I^{+/+} controls. Administration of reconstituted HDL (CSL-111) normalized hypothalamic inflammation and mitochondrial function markers in apoA-I^{-/-} mice. Treatment of primary astrocytes with apoA-I resulted in enhanced mitochondrial activity, implying that circulating HDL levels are likely important for astrocyte function. HDL-based therapies may consequently avert reactive gliosis in hypothalamic astrocytes by improving mitochondrial bioenergetics and thereby offering potential treatment and prevention for obesity and metabolic

disease.—Götz, A., M. Lehti, E. Donelan, C. Striese, S. Cucuruz, S. Sachs, C-X. Yi, S. C. Woods, S. D. Wright, T. D. Müller, M. H. Tschöp, Y. Gao, and S. M. Hofmann. **Circulating HDL levels control hypothalamic astrogliosis via apoA-I.** *J. Lipid Res.* 2018. 59: 1649–1659.

Supplementary key words mitochondria • inflammation • high density lipoprotein • apolipoprotein A-I • metabolism • dyslipidemia • adipose tissue • hypothalamus • astrocytes

Obesity is associated with a state of moderate but chronic inflammation that is characterized by increased tissue-specific levels, as well as circulating levels, of interleukins and cytokines, a condition that is thought to participate in the development of many obesity-associated comorbidities by inducing cellular dysfunction (1). Emerging evidence indicates that chronic consumption of excess calories induces inflammation in the arcuate nucleus (ARC) of the hypothalamus, a brain area important for the regulation of food intake and energy expenditure (2). This process is considered an early and determining factor for the onset of obesity because it occurs prior to body weight gain and

This work was supported by American Diabetes Association Grant 1-10-BS-72 and National Institutes of Health Grant 2K12HD051953-06. Additional partial support was provided by Deutsche Forschungsgemeinschaft Grant SFB1123-A4 and Helmholtz Alliance ICEMED (Imaging and Curing Environmental Metabolic Diseases) Grant WP 15 (to S.M.H.). The content is solely the responsibility of the authors and does not necessarily represent the official views of the National Institutes of Health.

Manuscript received 26 June 2018 and in revised form 9 July 2018.

Published, *JLR Papers in Press*, July 10, 2018
DOI <https://doi.org/10.1194/jlr.M085456>

Copyright © 2018 Götz et al. Published under exclusive license by The American Society for Biochemistry and Molecular Biology, Inc.

This article is available online at <http://www.jlr.org>

Abbreviations: A β , amyloid- β peptide; ARC, arcuate nucleus; BBB, blood-brain barrier; 2DG, 2-deoxy-glucose; ECAR, extracellular acidification rate; FCCP, carbonyl cyanide-4-(trifluoromethoxy)phenylhydrazine; GFAP, glial fibrillary acidic protein; Iba-1, ionized calcium-binding adaptor molecule 1; IL, interleukin; OCR, oxygen consumption rate; OXPHOS, oxidative phosphorylation; PGC1- α , peroxisome proliferator-activated receptor α coactivator 1 α ; PPR, proton production rate; rHDL, reconstituted HDL.

¹To whom correspondence should be addressed.

e-mail: susanna.hofmann@helmholtz-muenchen.de (S.M.H.);

yanqinggao@njmu.edu.cn (Y.G.)

^SThe online version of this article (available at <http://www.jlr.org>) contains a supplement.

participates in the development and progression of metabolic disorders including obesity, diabetes, and CVD. Mitochondrial activity, which is critical for proper functioning of the CNS, is compromised in inflammatory states, and there are documented molecular links among inflammation, impaired insulin signaling, and mitochondrial dysfunction in neurodegenerative diseases and diabetes (3). Novel therapeutic strategies may therefore be developed to target this impairment.

Within the hypothalamus, glial cells are key regulators of parenchymal homeostasis and neuronal communication. Glial cells become activated during periods of excess caloric intake, causing them to initiate inflammatory processes known collectively as reactive gliosis. As this occurs, the two main classes of glial cells, astrocytes and microglia, are converted to an activated pro-inflammatory phenotype characterized by cellular hypertrophy and proliferation, increased expression of intermediate filaments, and secretion of inflammatory interleukins and cytokines (2). Glial cells can also be activated directly by several pro-inflammatory factors or cytokines, including the metabolic hormone leptin, which stimulate the production of interleukin (IL)-1 β , TNF α , and IL-6 within the glial cells (4). Activated microglia and astrocytes continue to accumulate in the hypothalamus over months of excess caloric intake, such that hypothalamic inflammation becomes persistent, potentially leading to neuronal dysfunction and, thus, to a chronic impairment of energy homeostasis (5).

Epidemiological studies have confirmed a strong association between fat intake, plasma cholesterol levels, obesity, and CVD mortality (6, 7). One key independent predictor for CVD as well as for Alzheimer's dementia is a low level of HDL particles and their major protein constituent, apoA-I (8–10). Low circulating HDL and apoA-I are also a hallmark of obesity in association with insulin-resistance, a pathological precondition associated with T2D (11). HDLs have atheroprotective functions that are independent of their well-known role in lipid transport (12). In particular, HDLs directly mediate anti-inflammatory reprogramming of immune cells (13), promoting cerebrovascular health (10) and maintaining mitochondrial function [for review see (14)], activities that may prevent and/or ameliorate metabolic disease. However, it is not known whether circulating HDLs exert an independent effect on the development of obesity and metabolic dysfunction. We therefore investigated the role of genetically reduced HDL levels in the development of hypothalamic inflammation and mitochondrial dysfunction. Using a genetic loss of function mouse model (apoA-I^{-/-}), we report for the first time that low circulating HDL levels specifically promote astrocyte activation and induce mitochondrial dysfunction within the hypothalamic astrocytes that is associated with enhanced adiposity and impaired glucose homeostasis. Treatment of primary astrocytes with apoA-I results in enhanced mitochondrial bioenergetics of primary astrocytes, and administration of reconstituted HDL (rHDL) (CSL-111) in apoA-I^{-/-} mice reverses hypothalamic inflammation by normalizing mitochondrial function markers, suggesting that HDL-based therapies may avert astroglial dysfunction

and thus offer a new approach for potential treatment and prevention of obesity and metabolic disease.

MATERIALS AND METHODS

Animals

For phenotyping studies, apoA-I-deficient (apoA-I^{-/-}) male mice on the C57/BL/6J background (Jackson Laboratories, Bar Harbor, ME) were bred with female WT mice in our animal facilities. Age-matched male apoA-I^{-/-} mice and their WT male littermates (apoA-I^{+/+}) (n = 10–14 per group) were 6 months of age at the initiation of the study.

For pharmacological studies, reconstituted human HDL (CSL-111) was provided by CSL Behring AG (Bern, Switzerland) and prepared from human plasma as previously described (15). The preparation was supplied as a lyophilized powder that, upon reconstitution with sterile water, rendered a solution containing 19.5 g/l protein. The molar ratio protein-phospholipid was 1:155. Seven-month-old apoA-I^{-/-} male mice and WT mice (n = 6 per group) were randomized according to body weight and body composition. Mice were treated daily via intraperitoneal injections of CSL-111 (150 mg/kg) for 7 days during the light cycle. Vehicle mice received an equivalent volume of 0.9% saline.

All mice were housed in a pathogen-free environment on a 12:12 h light-dark cycle at 22°C with free access to food and water. Mice were fed a regular chow diet (5058 PicoLab Mouse Diet 20; LabDiet, Richmond, IN). Body fat mass was measured in conscious mice using 1H magnetic resonance spectroscopy (EchoMRI-100; Echo Medical Systems). All rodent studies were approved by and performed according to the guidelines of the Institutional Animal Care and Use Committee at the University of Cincinnati and the Helmholtz Center Munich.

Biochemical assays

Animals were fasted for 6 h prior to blood collection from the tail vein. Plasma cholesterol levels were determined using the Infinity cholesterol kit (Thermo Scientific Inc., Rockford, IL) as described (16). An intraperitoneal pyruvate tolerance test was conducted by injection of sodium pyruvate (2 g/kg; Sigma-Aldrich, St. Louis, MO) in 0.9% w/v NaCl, as described previously (17). Tail blood glucose levels (milligrams per deciliter) were measured with a TheraSense Freestyle glucometer (Abbott Diabetes Care, Inc., Alameda, CA) before (0 min) and at 15, 30, 45, 60, and 120 min after injection. Samples were analyzed individually except for lipoprotein separation, for which pooled samples were subjected to fast-performance LC, as described previously (16).

Brain cortex and liver lipid content of ad libitum-fed mice was assessed by extraction as described (16). Briefly, 20 mg of snap-frozen brain cortex and 50 mg of snap-frozen liver were homogenized with 1 ml chloroform. Lipids were extracted by overnight shaking at room temperature. For phase separation, 700 μ l of ddH₂O were added, samples were centrifuged at 775 g for 20 min at 4°C and the organic layer was collected. For the second extraction, 700 μ l of chloroform/methanol (2:1 v/v) were added to the remaining homogenate and lipid extraction, phase separation, and organic-layer collection were performed as described above. Fifteen microliters of both extractions were then transferred to glass tubes, evaporated, and measured with an Infinity cholesterol and triglyceride kit (Thermo Scientific Inc.).

Brain cortex tissue was snap-frozen for determination of citrate synthase activity by a colorimetric assay kit (K318-100; Biovision, Germany). Assay was carried out according to the manufacturer's instructions. Briefly, frozen tissues were homogenized with assay

buffer and incubated with substrate mix. Enzyme activity was calculated from standard curve. Protein level was determined by a Pierce BCA protein assay kit (Thermo Fisher, Germany). Citrate synthase activity was normalized to protein content.

Immunohistochemistry and quantitative analysis

At the termination of the study, mice were decapitated and brains were removed and immerse-fixed in 4% paraformaldehyde at 4°C for 24 h. Brains were then equilibrated for 48 h with 30% sucrose in 0.1 M TBS (pH 7.2). Immunohistochemistry and quantitative analysis for ionized calcium binding adaptor molecule 1 (Iba-1) and glial fibrillary acidic protein (GFAP) were performed on coronal brain sections (30 µm) throughout the hypothalamus as described previously (18). Briefly, after rinsing in 0.1 M TBS, whole-brain sections were incubated with rabbit anti-Iba-1 primary antibody (Synaptic Systems, Goettingen, Germany) at 1:1,000 dilution or rabbit anti-GFAP primary antibody (Dako, Carpinteria, CA) at 1:1,000 dilution overnight at 4°C. Sections were then rinsed and incubated with biotinylated secondary antibody (horse anti-rabbit IgG; Vector Laboratories, Burlingame, CA) for 1 h; subsequently, sections were rinsed and incubated in avidin-biotin complex (Vector Laboratories) for 1 h. The reaction product was visualized by incubation in 1% diaminobenzidine with 0.01% hydrogen peroxide for 1–10 min. Sections were mounted on gelatin-coated glass slides, dried, dehydrated in graded ethanol series, cleared in xylene, and cover-slipped for observation by light microscopy. All quantitative analyses were performed under blinded conditions and confirmed by at least two independent researchers. For each mouse, two to three sections in the middle portion of the ARC within the mediobasal hypothalamus were selected and images were captured by a computerized image analysis system consisting of an Axioskop color video camera (Carl Zeiss International, Thornwood, NY). Both sides of the ARC were manually outlined with an area of 0.04 mm² on each side. Immunoreactive cells were manually counted throughout the ARC and expressed as number of cells per square millimeter. The average from each mouse was then calculated and expressed as the mean ± SEM from each group.

Real-time PCR

Mice were euthanized by CO₂. Brains were subsequently harvested and hypothalami were immediately isolated and stored in liquid nitrogen. At a later time point, RNA was isolated by RNeasy lipid tissue mini kit (Qiagen, Hilden, Germany). After reverse transcription (QuantiTech reverse transcription kit; Qiagen), gene expression was analyzed by real-time PCR (ABI TaqMan 7900; Life Technologies GmbH, Darmstadt, Germany) using the company's reaction system and probes.

Cell culture

Hypothalami were isolated from 2-day-old male C57/BL/6J mice and triturated in MEM (Life Technologies GmbH) containing 1% penicillin-streptomycin, 10% FCS (Life Technologies GmbH), and 5.5 mM glucose. Astrocyte isolation was performed as described previously (19). The cell suspension was centrifuged for 7 min at 194 g and the pellet was resuspended and seeded in a 175 cm³ cell culture flask. Cells were incubated at 37°C and 5% CO₂ for 9 days with a regular medium change every 3 days. Prior to detachment, the flasks were placed in a 37°C shaking incubator at 280 rpm overnight. The cells were then washed and incubated for 2 min at 37°C with a 0.05% trypsin/EDTA solution (Biochrom AG, Berlin, Germany). Trypsinization was blocked with MEM + 10% FCS + 1% antibiotics. After centrifugation for 5 min at 194 g, supernatant was discharged and the cell pellet was resuspended in MEM + 10% FCS + 1% antibiotics and seeded in the XF24 plate with 80,000 cells per well (Seahorse Bioscience, North Billerica, MA).

Mitochondrial function analysis

Twenty-four hours after seeding, the medium was removed and primary astrocytes were washed with PBS before overnight incubation with MEM medium containing 20 µg/ml apoA-I (EMD Chemicals, Inc., San Diego, CA) or 20 µg/ml BSA (Sigma-Aldrich) in quintuplicates as reported (20). The next morning, cells were washed with PBS and incubated with XF assay medium containing 5.5 mM glucose for 1 h in a 37°C air incubator. The XF24 plate was then transferred to a temperature-controlled (37°C) Seahorse (extracellular flux) analyzer (Seahorse Bioscience) and subjected to an equilibration period. Respirometry analysis was performed as described previously (21). Briefly, one assay cycle consisted of a 1 min mix, 2 min wait, and 3 min measurement period. After four basal assay cycles, oligomycin (20 µg/ml) was added by automatic pneumatic injection to inhibit ATP synthase for the determination of the proportion of respiration used to drive ATP synthesis for three additional cycles. Subsequently, carbonyl cyanide-4-(trifluoromethoxy)phenylhydrazone (FCCP; 10 µM) was added the same way to determine maximal respiration in mitochondria by uncoupling ATP synthesis from electron transport for another three assay cycles. Finally, rotenone (25 µM) plus antimycin A (25 µM) was added to determine the nonmitochondrial respiratory rate in the next three assay cycles, which was then subtracted from all other rates. Oxygen consumption rate (OCR) traces and a scheme about the different modules that we analyzed are depicted in Fig. 3. Coupling efficiency was calculated as the oligomycin-sensitive fraction of mitochondrial respiratory activity. ATP production from oxidative phosphorylation (OXPHOS) was calculated using a phosphate/oxygen ratio of 2.3 (22). For analysis of extracellular acidification rates (ECARs) derived from glycolysis, measurements were ended by addition of 2-deoxy-glucose (2DG; 100 mM). ECAR traces and the different modules that we analyzed are depicted in Fig. 4. ECARs were converted into proton production rates (PPRs) by taking into account the buffer capacity. The 2DG-sensitive PPR estimates ATP production from glycolysis with a 1:1 ratio. To normalize respirometry readings to cell number per well, cells were stained with crystal violet after the flux experiment in the Seahorse XF analyzer. Briefly, cells were fixed with 4% paraformaldehyde for 30 min at room temperature. After washing three times with PBS, 200 µl of 0.1% crystal violet were added into each well and incubated for 10 min. After incubation time, crystal violet was removed and the plate was rinsed with distilled water. When the plate was completely dry, 500 µl of 10% acetic acid were added into each well. Absorbance was read at 590 nm.

Statistical analysis

Quantitative data are presented as mean ± SEM. Values were analyzed for statistically significant differences applying two-tailed unpaired *t*-tests for comparisons between untreated apoA-I^{+/+} and apoA-I^{-/-} mice and one-way or two-way ANOVA tests for CSL treatment comparisons between apoA-I^{+/+} and apoA-I^{-/-} mice, as recommended by GraphPad Prism for optimal analysis. Data homogeneity was analyzed by Bartlett's test and F test, accordingly. *P* < 0.05 was considered significant (GraphPad Prism, GraphPad Software, La Jolla, CA; SigmaStat, Systat Software, San Jose, CA).

RESULTS

Mice with markedly reduced circulating HDLs exhibit enhanced astroglia associated with increased IL-6 expression in the ARC

To determine whether circulating HDL levels modulate hypothalamic inflammation, we used a genetic loss of

function mouse model for apoA-I (apoA-I^{-/-}), the main protein component of HDL. As expected, fast-performance LC analysis of apolipoprotein profiles revealed a severely reduced circulating HDL cholesterol concentration in apoA-I^{-/-} mice compared with WT littermates (apoA-I^{+/+}; Fig. 1A, B). We found that in the absence of apoA-I, mRNA levels of the inflammatory IL-6 were significantly increased in the hypothalamus (Fig. 1C). GFAP is an intermediate filament protein that reliably identifies reactive astrocytes in association with cell process expansion (23, 24). Using immunohistochemical staining of brain sections for GFAP, we found that astrocytic gliosis is markedly increased specifically in the ARC of apoA-I^{-/-} compared with apoA-I^{+/+} mice (Fig. 1D). Consistent with increased reactive astrocytosis, we also found that the GFAP-labeled cells were enlarged in size and had more extensive processes, thus exhibiting the typical pro-inflammatory morphology. In parallel, we determined whether ARC microglial cells were activated by immunohistochemistry using the well-established macrophage/microglia-specific marker, ionized calcium-binding adapter molecule 1 (Iba-1) (25). Iba-1 is specifically expressed in activated microglia and is thus regarded as a specific surrogate parameter for microgliosis. It has been commonly used to detect and compare activated microglia in numerous species (26). Our quantitative analysis of brain sections revealed no differences in microglial activation in the ARC between the two genotypes (Fig. 1E). As an additional sign of microglial activation,

Iba-1-positive cells display the typical pro-inflammatory morphology of enlarged cell bodies and thickened processes. Herein, we observed no difference in morphology of microglia in the hypothalami of apoA-I^{-/-} compared with apoA-I^{+/+} mice. In other regions of the brain, including the hippocampus or the cortex, we did not observe differences in astroglial and microglial activation (supplemental Fig. S1A, B). In conclusion, our results indicate that circulating HDLs associate with reactive astroglial activation in the ARC, an area known to play a pivotal role in the regulation of energy balance.

Low circulating HDL levels are associated with increased adiposity, hepatic steatosis, and impaired glucose homeostasis in mice fed a low-fat diet

To understand whether the increased reactive astrocytosis observed in apoA-I^{-/-} mice is associated with early markers of metabolic dysfunction, we determined body composition and circulating glucose levels in apoA-I^{-/-} and apoA-I^{+/+} mice. Although apoA-I^{-/-} mice had similar body weights as apoA-I^{+/+} mice when fed a regular chow diet, we confirmed previous results by us and others showing that absence of apoA-I in mice results in increased fat mass (27) (Fig. 2A, B). Hepatic triglyceride content was also markedly increased in apoA-I^{-/-} compared with apoA-I^{+/+} mice (Fig. 2C), indicating that the excess body fat mass in apoA-I^{-/-} mice results, in part, from an increased triglyceride accumulation within the liver. We next asked

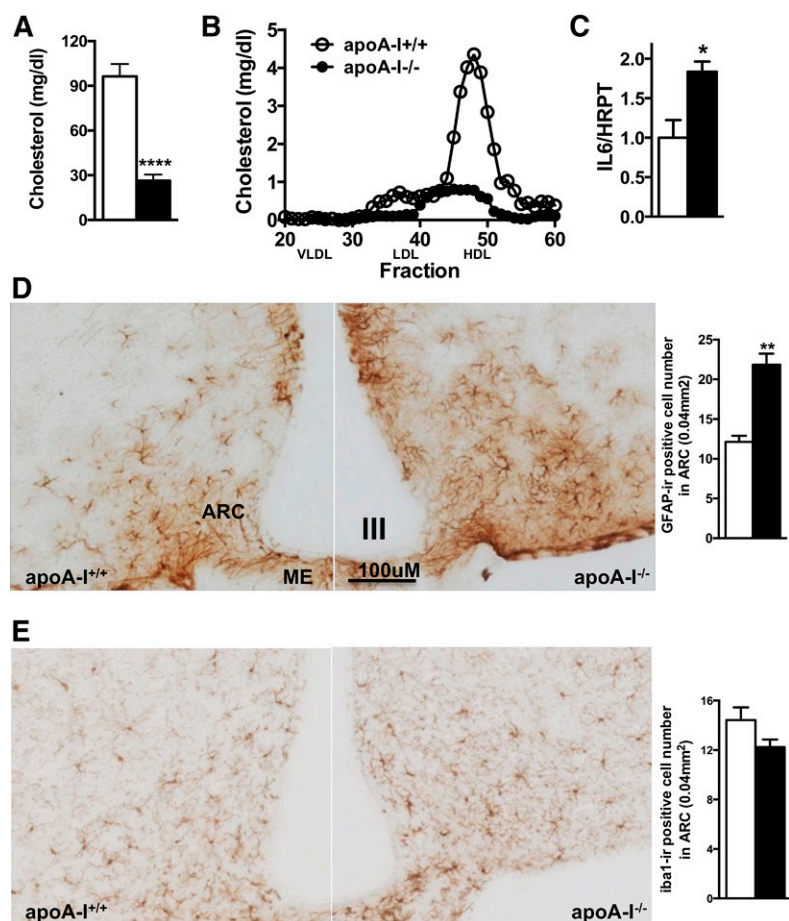


Fig. 1. Reactive astroglial activation is enhanced in the hypothalamic ARC of mice with genetically reduced HDL levels. Total circulating cholesterol levels (A) and HDL particle concentration (B) are markedly reduced in apoA-I-deficient mice (apoA-I^{-/-}; closed bars; closed circles) compared with WT mice fed a normal chow diet (apoA-I^{+/+}; open bars; open circles) (n = 8 mice). IL-6 mRNA levels are significantly increased in hypothalami of apoA-I^{-/-} (closed bar) compared with apoA-I^{+/+} mice (open bar) (C). GFAP-immunopositive cells in the ARC of apoA-I-deficient mice are significantly increased compared with levels in WT mice (D), but not Iba-1 immunopositive cells (E). ME, median eminence; III, third ventricle. Data are expressed as mean ± SEM. *P < 0.05, **P < 0.005; ****P < 0.00005 versus WT mice.

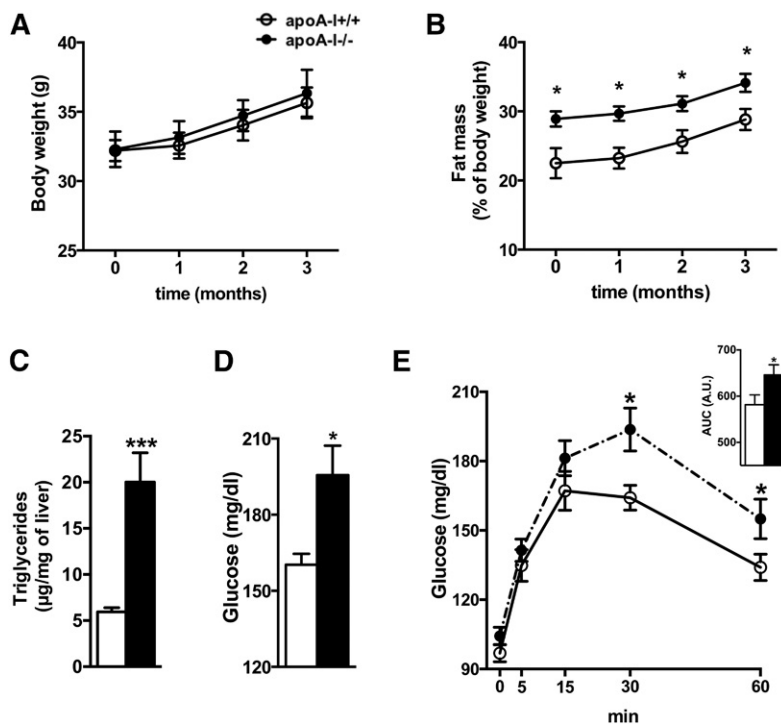


Fig. 2. Mice with low circulating HDL levels exhibit signs of metabolic disease. Body composition analysis revealed similar body mass (A), but increased fat mass (B), in apoA-I-deficient mice (closed circles) compared with WT littermates (open circles). Liver triglyceride content (C), fasting glucose levels (D), and hepatic glucose output measured by the pyruvate tolerance test (E) were significantly increased in apoA-I-deficient mice (closed bars) compared with levels in WT littermates (open bars). Data are expressed as mean \pm SEM. * $P < 0.05$; *** $P < 0.0005$ versus WT mice.

whether the hepatic steatosis in apoA-I^{-/-} mice is associated with impaired hepatic glucose homeostasis. As depicted in Fig. 2D, fasting glucose levels were significantly higher in apoA-I^{-/-} compared with apoA-I^{+/+} mice, implying deterioration of hepatic glucose metabolism. Consistent with the latter, glucose measurements during a pyruvate tolerance test also revealed an enhanced hepatic glucose output in apoA-I^{-/-} mice compared with their apoA-I^{+/+} littermates (Fig. 2E). These findings suggest that apoA-I deficiency contributes to impaired hepatic lipid and glucose homeostasis.

apoA-I directly enhances cellular respiration by increasing mitochondrial fluxes in primary astrocytes

To determine whether HDL and apoA-I have a direct effect on the cellular bioenergetics of primary astrocytes, we measured OCR using a Seahorse XF24 extracellular flux analyzer. For the analysis of the oxygen-consuming processes, we sequentially added inhibitors of the mitochondrial transport chain. **Figure 3A** depicts the time-lapse measurements of OCRs in absolute values, which can be divided into distinct modules of oxygen consumption and mitochondrial and cellular processes (Fig. 3B). Our analysis revealed that cellular respiration was increased significantly in primary astrocytes upon incubation with apoA-I relative to astrocytes incubated with BSA (Fig. 3A, C), implying enhanced mitochondrial activity in cells treated with apoA-I. To further dissect whether this increase in cellular respiration is due to increases in mitochondrial and/or nonmitochondrial respiration, we used rotenone (complex I inhibitor) and antimycin A (complex III inhibitor) at the end of the experiment to completely inhibit mitochondrial fluxes (Fig. 3B). As depicted in Fig. 3A and C, basal mitochondrial respiration was increased in astrocytes

treated with apoA-I compared with BSA-treated cells, suggesting that apoA-I induces a higher ATP turnover and demand. Using the ATP synthase inhibitor, oligomycin, we determined that both ATP-linked respiration and proton leak are higher in apoA-I-treated cells relative to cells treated with BSA (Fig. 3D). Using the protonophore, FCCP, for the induction of maximal substrate oxidation, we further determined that the maximal ATP output, which is controlled by substrate oxidation capacity, is not significantly increased in apoA-I-treated astrocytes compared with BSA-treated cells (Fig. 3E). Our analysis of spare respiratory capacity determined by subtracting basal respiration from FCCP-induced respiration also revealed no differences between the cells treated with apoA-I or BSA (Fig. 3E). Mitochondrial efficiency, also termed coupling efficiency, was similar between astrocytes treated with apoA-I and BSA. Taken together, the higher cellular respiration of astrocytes treated with apoA-I can be attributed to apoA-I-enhanced mitochondrial respiration.

apoA-I reduces maximal glycolytic capacity in primary astrocytes

To determine whether apoA-I also induces changes in cytoplasmic glycolysis, the ATP source complementary to mitochondria, we compared ECARs in primary astrocytes incubated with apoA-I or BSA simultaneously to OCR (Fig. 4A). As occurred with OCR, we characterized glycolysis in more detail with the use of specific inhibitors. Nonglycolytic acidification was determined by adding 2DG, an inhibitor of glycolysis (Fig. 4B). Astrocytes treated with apoA-I had lower cellular acidification values than BSA-treated astrocytes (Fig. 4C). While nonglycolytic acidification rates were comparable between astrocytes treated with apoA-I or BSA, basal glycolytic rates were lower in apoA-I-treated

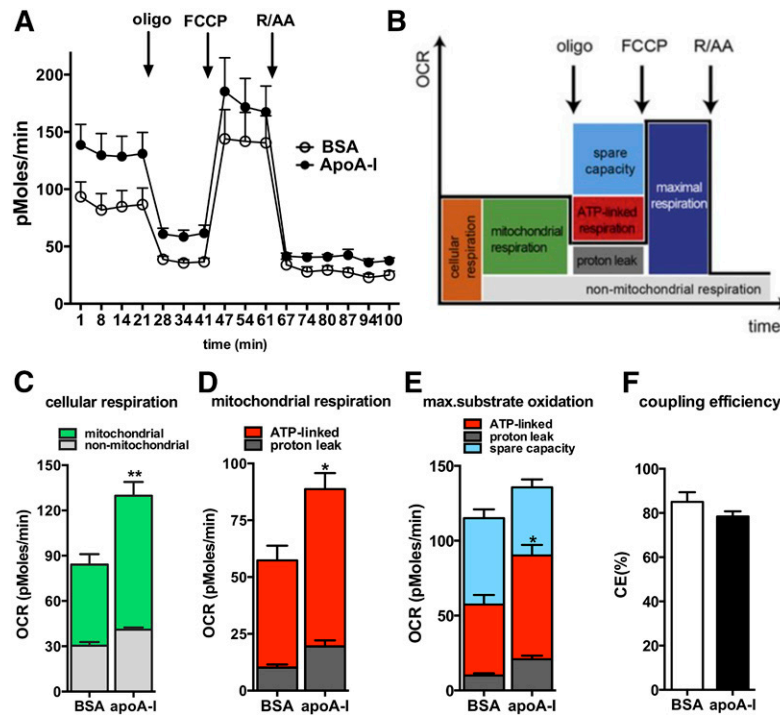


Fig. 3. apoA-I directly enhances cellular respiration by increasing mitochondrial activity in primary astrocytes. Cellular respiration and respiration after interference of mitochondrial pathways with specific inhibitors was analyzed in astrocytes incubated with BSA or apoA-I (20 μ g/ml overnight) using an XF24 extracellular flux analyzer as described in the Materials and Methods. A: OCR over time in primary astrocytes treated with apoA-I (filled circles) and BSA (open circles). B: Scheme defining the oxygen-consuming processes of a cell. C: Cellular respiration was dissected into mitochondrial (green) and nonmitochondrial (gray) respiration using the electron transfer chain inhibitors, rotenone (R; 25 μ M) and antimycin A (AA; 25 μ M). D: Mitochondrial respiration was further dissected into proton leak (dark gray) and ATP-linked respiration (red) using the ATP-synthase inhibitor, oligomycin (oligo; 20 μ g/ml). E: Maximal respiration (dark blue) of astrocytes after addition of the chemical uncoupler, FCCP (10 μ M), and after subtracting nonmitochondrial respiration rates. The portion of spare respiratory capacity (light blue) was determined by subtracting basal respiration from maximal respiration rates. F: Mitochondrial coupling efficiencies were calculated as the fraction of mitochondrial oxygen consumption that is sensitive to oligomycin, reflecting the fraction used to drive ATP synthesis. AU, arbitrary units. All data are expressed as mean \pm SEM of five replicates run in parallel. * P < 0.05, ** P < 0.005.

astrocytes (Fig. 4C). The difference in basal glycolytic ECARs of astrocytes treated with apoA-I, as compared with astrocytes treated with BSA, indicates reduced glycolytic ATP production in astrocytes treated with apoA-I. Consistent with the latter, we detected a marked decrease in glycolytic activity when we induced maximal glycolytic rates by inhibiting mitochondrial ATP production with oligomycin (Fig. 4D).

apoA-I increases the ATP demand fueled by OXPHOS

To better characterize ATP homeostasis in astrocytes treated with apoA-I, we determined ATP production by OXPHOS within the mitochondria and ATP production by glycolysis within the cytoplasm. Our calculation (described in the Materials and Methods section) of the flux data indicates higher mitochondrial ATP output (Fig. 4E) and lower glycolytic ATP production (Fig. 4F) in apoA-I-treated astrocytes as compared with BSA-treated astrocytes, resulting in a slightly higher, but not significant, total ATP turnover in apoA-I-treated cells (Fig. 4G). Calculating the proportions of ATP production from OXPHOS and glycolysis demonstrated that regardless of treatment, astrocytes utilized

mainly OXPHOS processes to fuel their demand for ATP (Fig. 4H). apoA-I treatment significantly increases the percentage of mitochondrial ATP production contributing to total ATP production in primary astrocytes.

CSL-111 treatment normalizes hypothalamic inflammation and mitochondrial function markers in chow-fed apoA-I^{-/-} mice

To test the effect of rHDL on hypothalamic inflammation, groups of 7-month-old male apoA-I^{-/-} and apoA-I^{+/+} C57BL/6J mice were randomized according to body weight and body composition and treated once daily via intraperitoneal injection of CSL-111 (150 mg/kg) or an equivalent volume of saline (vehicle group) for seven consecutive days. In line with our previous findings, analysis of circulating cholesterol levels and apolipoprotein profiles revealed a severely reduced circulating HDL particle concentration in apoA-I^{-/-} compared with apoA-I^{+/+} mice, which completely normalized after a week of CSL-111 treatment (Fig. 5A, B). Confirming our previous results (Fig. 1C, D), deficiency in apoA-I enhances hypothalamic mRNA levels of IL-6 and the astrocyte-specific marker, GFAP, while not

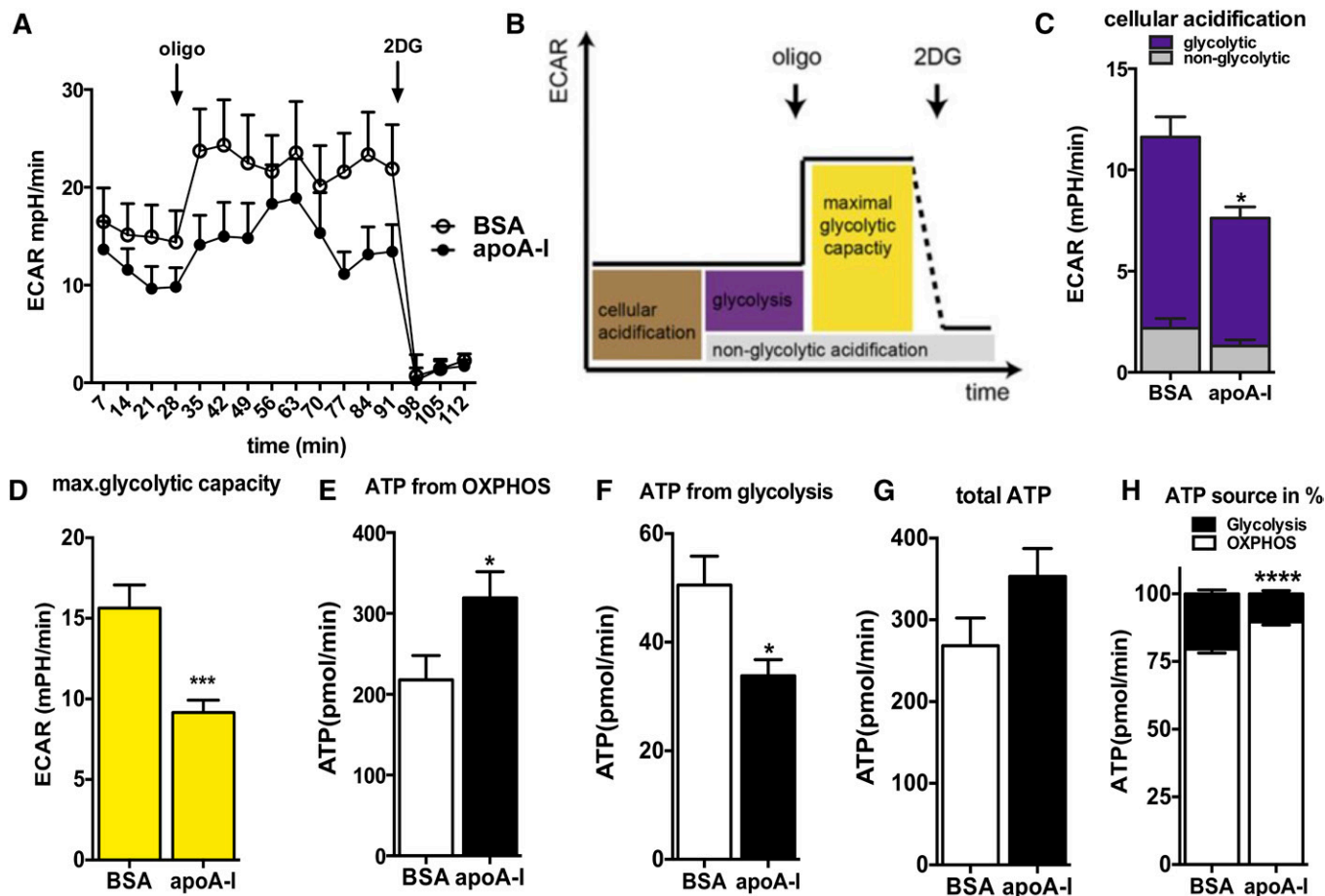


Fig. 4. apoA-I reduces glycolytic activity in primary astrocytes and enhances ATP demand fueled by OXPHOS. **A:** The ECAR was recorded simultaneously with the OCR of astrocytes incubated with BSA or apoA-I (20 μ g/ml overnight) with a Seahorse XF96 extracellular flux analyzer, as described in the Materials and Methods. **B:** Scheme defining cellular ECAR processes. Data after FCCP and rotenone/antimycin A injection were not used for ECAR analysis. **C:** By inhibiting glycolysis with 2DG (100 mM) as the last step in the measurements, cellular acidification was broken down to nonglycolytic acidification (gray) and acidification due to glycolysis (purple). **D:** By inhibiting mitochondrial ATP synthesis with oligomycin, the maximal glycolytic capacity was obtained. **E:** ATP production rates of OXPHOS pathways of BSA-treated (open bar) and apoA-I-treated (closed bar) primary astrocytes. **F:** ATP production rates of glycolysis as estimated via PPRs of BSA-treated (open bar) and apoA-I-treated (closed bar) primary astrocytes. **G:** Sum of ATP produced by OXPHOS and glycolysis of BSA-treated (open bar) and apoA-I-treated (closed bar) primary astrocytes. **H:** Percentage of OXPHOS (closed bars) and glycolytic (open bars) ATP production on total ATP production in BSA- and apoA-I-treated primary astrocytes. Data are expressed as the mean \pm SEM of five replicates run in parallel. * $P < 0.05$, *** $P < 0.0005$, **** $P < 0.00005$.

modifying levels of the microglial specific marker, Iba-1 (Fig. 5C). Administration of CSL-111 for 7 days normalizes these hypothalamic inflammation markers in apoA-I^{-/-} mice fed a chow diet (Fig. 5C).

Citrate synthase is an enzyme exclusively present in the mitochondrial matrix and thus a quantitative marker for the presence of intact mitochondria. Our quantitative analysis of citrate synthase activity revealed significantly increased levels in the CNS of CSL-111-treated apoA-I^{-/-} mice (Fig. 5D), thus revealing enhanced mitochondrial density after treatment with CSL-111. Mitochondrial energy-transducing capacity is essential for maintenance of cellular function and impaired mitochondrial energy metabolism is a hallmark of different inflammatory diseases (3). As a next step, we determined whether CSL-111 treatment also affects different mitochondrial markers connected to mitochondrial biogenesis, fusion, and OXPHOS. We found that the mRNA levels of PPARc coactivator 1 α (Pgc1 α) (master

regulator of mitochondrial biogenesis), ATP synthase subunit β (Atp5b) and cytochrome C1 (Cyc1) (both enzymes involved in OXPHOS), mitofusin 2 (Mit2; one key enzyme involved in mitochondrial fusion), and optic atrophy 1 (Opa1; mitofusion regulatory gene) were all increased in apoA-I^{-/-} mice compared with apoA-I^{+/+} mice and that CSL-111 normalized all of these markers in apoA-I^{-/-} mice (Fig. 5E).

CSL-111 treatment reduced fat mass in both apoA-I^{+/+} and apoA-I^{-/-} mice (Fig. 5F). However, different tissues of apoA-I^{-/-} and apoA-I^{+/+} mice were affected by this decrease in body fat. In apoA-I^{+/+} mice, the reduction was mainly visible in visceral fat (Fig. 5G); while in apoA-I^{-/-} mice, the reduction was mainly in the liver (Fig. 5H, I) and the brain (Fig. 5J, K). CSL-111 treatment further seemed to normalize lean mass increase in apoA-I^{-/-} mice (Fig. 5F). We further observed increased amounts of cholesterol and triglycerides in the brains of apoA-I^{-/-} mice (Fig. 5J)

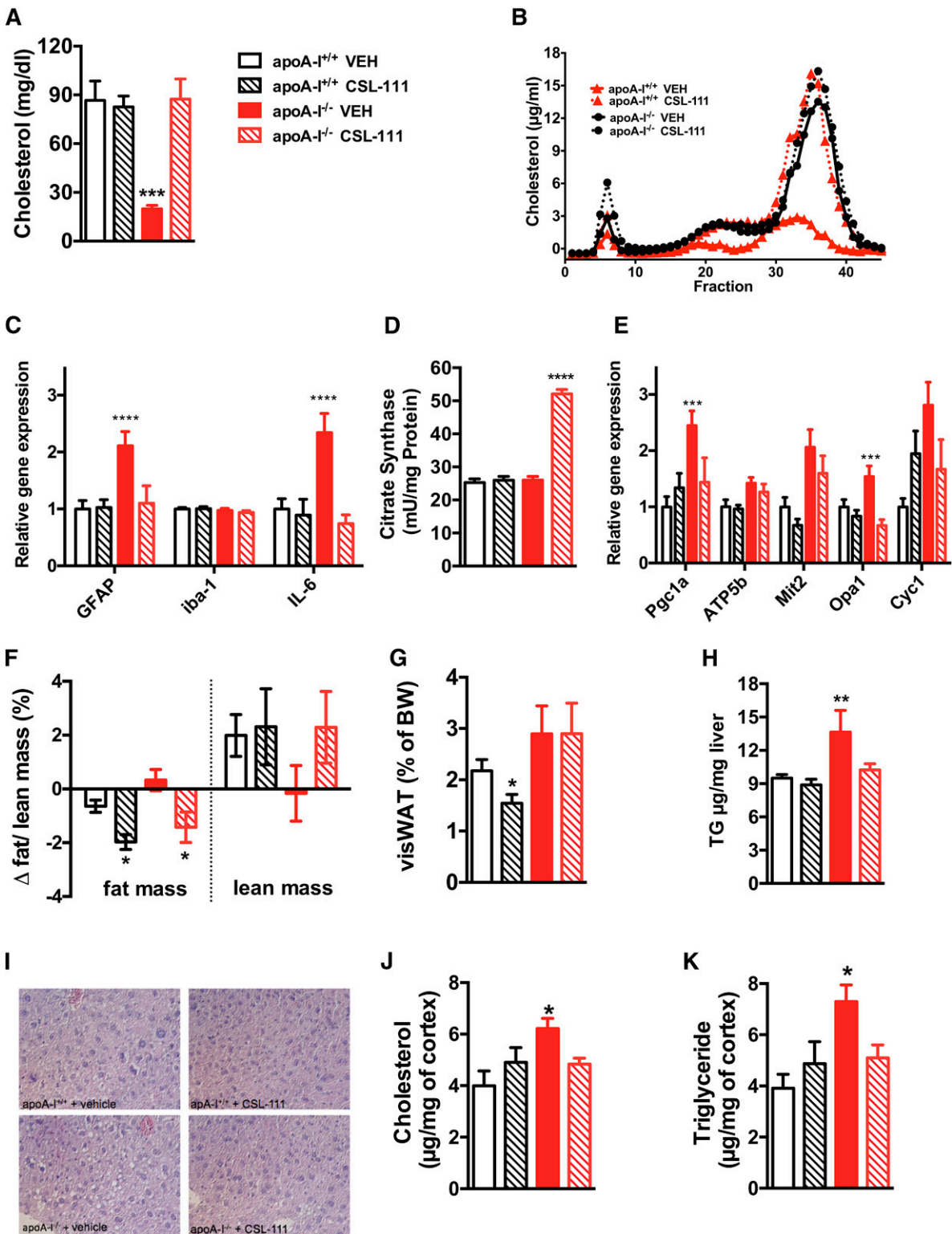


Fig. 5. CSL-111 treatment normalizes hypothalamic inflammation and mitochondrial function markers in chow-fed apoA-I^{-/-} mice. Plasma total cholesterol levels (A) and lipoprotein fractions (B) of apoA-I^{+/+} and apoA-I^{-/-} mice after daily treatment with CSL-111 at 150 mg/kg for 7 days (n = 6 mice per group, age 7 months). CSL-111 normalizes hypothalamic inflammation (C) and reverses mitochondrial changes by enhancing citrate synthase activity (D) and normalizing mitochondrial function markers (E) in apoA-I^{-/-} mice. Body composition analysis revealed reduced fat mass in apoA-I^{+/+} (white hatched bars) and apoA-I^{-/-} mice (red hatched bars) treated with CSL-111 compared with vehicle-treated groups (F). The changes in body composition were due to reduced visceral fat mass in apoA-I^{+/+} mice (white hatched bars) (G) and due to reduced hepatic fat content in apoA-I^{-/-} mice (red hatched bars) (H). Representative pictures of H&E-stained hepatic sections from WT and apoA-I^{-/-} mice revealed accumulation of hepatic lipids in the form of lipid droplets within the hepatocytes in vehicle-treated apoA-I^{-/-} mice (40× magnification), which normalized in the CSL-111 treatment group. CSL-111 treatment normalized cholesterol (J) and triglyceride (K) levels in the CNS of apoA-I^{-/-} mice. Data are expressed as mean ± SEM. **P* < 0.05, ***P* < 0.005, ****P* < 0.0005, *****P* < 0.00005 versus apoA-I^{+/+} mice. Atp5b, ATP synthase subunit β; Cyc1, cytochrome C1; Mit2, mitofusin 2; Opa1, optic atrophy 1; Pgc1α, PPARc coactivator 1α.

compared with apoA-I^{+/+} mice. Treatment with CSL-111 normalized both in apoA-I^{-/-} mice without affecting lipid levels in the brains of apoA-I^{+/+} mice (Fig. 5J, hatched bars). Changes in brain cholesterol levels in mice treated with CSL-111 were associated with modest and not significant changes in RNA expression levels of transporters and enzymes involved in cholesterol transport (supplemental Fig. S2).

DISCUSSION

Our data presented herein show that circulating HDL levels affect astrocyte function in the region of the hypothalamus, a brain region important for energy balance. We report, for the first time to our knowledge, that deficiency of apoA-I results in hypothalamic astrogliosis that is associated with impaired metabolic homeostasis and that administration of rHDL (CSL-111) normalizes hypothalamic inflammation and mitochondrial function. Because our observations were made in mice consuming a chow diet with a very low content of fat (9%), they suggest that low circulating HDL levels directly induce hypothalamic astrocyte dysfunction and metabolic disease, even in the absence of caloric excess. In view of the well-established strong correlation of low HDL and insulin resistance (28), our data imply that individuals with low HDL levels per se have an increased risk for the development of metabolic disease. More importantly, our observations support an emerging paradigm that impairment of HDL function could play a direct role in the pathogenesis of T2D.

We observed a marked and specific activation of astrocytes in the absence of apoA-I, with no change in microglial cell status. This is particularly interesting because it has become increasingly clear that astrocytes, the most abundant glial cell type in the mammalian brain, are critical to essential CNS actions, including synaptic transmission, regulation of neural immune responses, antioxidant defense, structural and nutritive support of neurons, and neuronal survival (29). More importantly, recent research has implicated hypothalamic astrocytes as crucial players in the homeostatic control of metabolism by the brain, partly due to their strategic location close to the blood-brain barrier (BBB) (30). Consistent with this, Kim et al. (31) detected an active role of astrocytes in the initiation of hypothalamic synaptic plasticity and neuroendocrine control of feeding by leptin. The fact that reactive astrogliosis has been detected in the hypothalamus of high-fat diet-induced obese rodents, even before weight gain (5, 32), points to its pivotal role in the pathogenesis of metabolic disease. Our intriguing observation that hypothalamic astrogliosis is enhanced in apoA-I-deficient mice fed a low-fat diet and is associated with the classical signs of metabolic disease may thus provide further evidence for the important role of astrocytes in metabolic control and obesity.


Recent work has indicated that circulating HDLs are important for a well-functioning BBB by promoting cerebrovascular health through several mechanisms. For example, entering the CNS via the choroid plexus (33), HDL may

maintain BBB integrity from the luminal side of the vessel by promoting repair of damaged endothelial cells and enhancing endothelial integrity and barrier function. HDL may also prevent deleterious amyloid- β peptide (A β) accumulation by enhancing its clearance from the brain and accelerating its degradation. Consistent with the latter, several investigators have demonstrated in vitro that apoA-I inhibits A β aggregation into fibrils and reduces A β -induced cytotoxicity, oxidative stress, and neuronal degeneration [for review see (10)]. Thus, there is an increasing effort underway to utilize these beneficial effects of HDLs for the treatment of Alzheimer's disease. For example, it has recently been reported that treatment with HDL-based nanoparticles resulted in decreased A β deposition, attenuated reactive gliosis, ameliorated neurological alterations, and reduced memory deficits in an animal model of Alzheimer's disease (34). Most importantly, previous data have shown that apoA-I protects mitochondria by multiple mechanisms involving interaction with CoQ₁₀ to stabilize complex II and inhibit reactive oxygen species-mediated damage to respiratory complexes (14). It seems plausible that these mechanisms may contribute to the herein observed improvement of mitochondrial bioenergetics by administration of HDL particles. In addition, a putative link has been developed in recent years between major players involved in HDL-mediated cholesterol reuptake, like ABCA1, endocytosis, and mitochondrial metabolism (34), but the detailed underlying mechanisms are still unknown. RNA expression data from our study corroborate this link, and investigations led by us and others are ongoing to fully understand this novel HDL function. Consistent with our observation that HDLs modify mitochondrial bioenergetics in the hypothalamus is the evidence that administration of bezafibrate, a fibrate drug used to lower LDL cholesterol and increase HDL cholesterol levels in the blood, resulted in an increase in mitochondrial proteins and mitochondrial ATP-generating capacity (35). Importantly, bezafibrate treatment also attenuated astrogliosis and reduced inflammatory marker levels. Similarly, administration of rHDL (CSL-111) reverses reactive astrogliosis and mitochondrial dysfunction in the hypothalamus of apoA-I^{-/-} mice. Collectively, our data reveal that CSL-111 treatment may offer therapeutic potential to correct diet-independent alterations in the functional integrity of hypothalamic astrocytes by targeting pathways connecting inflammation and mitochondrial homeostasis.

Our finding that apoA-I directly improves mitochondrial activity in primary astrocytes further supports the hypothesis that HDLs are important in astrocyte function. Although we and others have clearly demonstrated that apoA-I directly modulates metabolism of different cell types within the CNS, it is still unclear how apoA-I-containing lipoprotein particles may exert these direct effects in vivo, considering that apoA-I is not produced by glial or neuronal cells within the brain and the BBB may exclude HDL particles from entering from the circulation. It has been hypothesized that apoA-I may be transported from the blood directly across the BBB [for review see (35)], and research is ongoing to determine whether pathways similar to its transport

in peripheral endothelial cells are involved (36, 37). Even without such a pathway, HDL may be able to reach the cells studied here, given the structural differences of the BBB in the hypothalamus and its greater permeability of this barrier to macromolecules (38). The ongoing debate whether apoA-I proteins cross the BBB is a prominent lack of knowledge due to potential clinical implications, one of which we report herein. Understanding how circulating proteins like apoA-I are entering the brain is of pivotal importance for the development of drugs that target specific brain areas important for metabolic control.

Although elevated HDL cholesterol levels in the blood represent one of the strongest epidemiological surrogates for protection against CVD, recent human genetic and pharmacological intervention studies have raised controversy about the causality of this relationship [for review see (39)]. Collectively, all these data indicate that HDL cholesterol concentration in the blood is only giving a static snapshot of a very dynamic and heterogeneous metabolic milieu and is thus unlikely itself causally protective against CVD. It seems more plausible that HDL function is a better predictor of CVD compared with its simple level in the blood, as has been repeatedly shown by several independent groups (40, 41)

In conclusion, our results point to a novel role of HDLs in maintaining normal hypothalamic function. Circulating HDLs and their major protein component, apoA-I, have several beneficial functions for brain cell metabolism, including effects on endothelial repair, inflammation, A β metabolism, and cognitive function, and all of these suggest an HDL-based therapy as a potential treatment for metabolic disease. Because chronic inflammatory diseases like obesity, T2D, and CVD affect cerebrovascular health (42), it is important to understand whether infusion of HDL particles from healthy subjects may prevent or repair cerebrovascular damage and thus improve metabolic function. 

Note added in proof

Timo Müller was inadvertently omitted as an author in the version of this article that was published as a Paper in Press on July 10, 2018. This error has now been corrected.

REFERENCES

- Hotamisligil, G. S. 2010. Endoplasmic reticulum stress and the inflammatory basis of metabolic disease. *Cell*. **140**: 900–917.
- Kälén, S., F. L. Heppner, I. Bechmann, M. Prinz, M. H. Tschöp, and C. X. Yi. 2015. Hypothalamic innate immune reaction in obesity. *Nat. Rev. Endocrinol.* **11**: 339–351.
- De Felice, F. G., and S. T. Ferreira. 2014. Inflammation, defective insulin signaling, and mitochondrial dysfunction as common molecular denominators connecting type 2 diabetes to Alzheimer disease. *Diabetes*. **63**: 2262–2272.
- Buckman, L. B., and K. L. J. Ellacott. 2014. The contribution of hypothalamic macroglia to the regulation of energy homeostasis. *Front. Syst. Neurosci.* **8**: 212.
- Thaler, J. P., C. X. Yi, E. A. Schur, S. J. Guyenet, B. H. Hwang, M. O. Dietrich, X. Zhao, D. A. Sarruf, V. Izgur, K. R. Maravilla, et al. 2012. Obesity is associated with hypothalamic injury in rodents and humans. *J. Clin. Invest.* **122**: 153–162.
- Rees, K., M. Dyakova, N. Wilson, K. Ward, M. Thorogood, and E. Brunner. 2013. Dietary advice for reducing cardiovascular risk. *Cochrane Database Syst. Rev.* **12**: CD002128.
- Hooper, L., C. D. Summerbell, R. Thompson, D. Sills, F. G. Roberts, H. J. Moore, and G. Davey Smith. 2012. Reduced or modified dietary fat for preventing cardiovascular disease. *Cochrane Database Syst. Rev.* **5**: CD002137.
- Boden, W. E. 2000. High-density lipoprotein cholesterol as an independent risk factor in cardiovascular disease: assessing the data from Framingham to the Veterans Affairs High-Density Lipoprotein Intervention Trial. *Am. J. Cardiol.* **86**: 19L–22L.
- McNeill, A. M., K. Katz, C. J. Girman, W. D. Rosamond, L. E. Wagenknecht, J. I. Barzilay, R. P. Tracy, P. J. Savage, and S. A. Jackson. 2006. Metabolic syndrome and cardiovascular disease in older people: the cardiovascular health study. *J. Am. Geriatr. Soc.* **54**: 1317–1324.
- Stukas, S., J. Robert, and C. L. Wellington. 2014. High-density lipoproteins and cerebrovascular integrity in Alzheimer's disease. *Cell Metab.* **19**: 574–591.
- ACCORD Study Group, H. N. Ginsberg, M. B. Elam, C. L. Lovato, J. R. Crouse, L. A. Leiter, P. Linz, W. T. Friedewald, J. B. Buse, H. C. Gerstein, et al. 2010. Effects of combination lipid therapy in type 2 diabetes mellitus. *N. Engl. J. Med.* **362**: 1563–1574.
- Kingwell, B. A., M. J. Chapman, A. Kontush, and N. E. Miller. 2014. HDL-targeted therapies: progress, failures and future. *Nat. Rev. Drug Discov.* **13**: 445–464.
- De Nardo, D., L. I. Labzin, H. Kono, R. Seki, S. V. Schmidt, M. Beyer, D. Xu, S. Zimmer, C. Lahrmann, F. A. Schildberg, et al. 2014. High-density lipoprotein mediates anti-inflammatory reprogramming of macrophages via the transcriptional regulator ATF3. *Nat. Immunol.* **15**: 152–160.
- White, C. R., G. Datta, and S. Giordano. 2017. High-density lipoprotein regulation of mitochondrial function. *Adv. Exp. Med. Biol.* **982**: 407–429.
- Lerch, P. G., V. Förtsch, G. Hodler, and R. Bolli. 1996. Production and characterization of a reconstituted high density lipoprotein for therapeutic applications. *Vox Sang.* **71**: 155–164.
- Hofmann, S. M., L. Zhou, D. Perez-Tilve, T. Greer, E. Grant, L. Wancata, A. Thomas, P. T. Pfluger, J. E. Basford, D. Gilham, et al. 2007. Adipocyte LDL receptor-related protein-1 expression modulates postprandial lipid transport and glucose homeostasis in mice. *J. Clin. Invest.* **117**: 3271–3282.
- Habegger, K. M., D. Matzke, N. Ottaway, J. Hembree, J. Holland, C. Raver, J. Mansfeld, T. D. Müller, D. Perez-Tilve, P. T. Pfluger, et al. 2012. Role of adipose and hepatic atypical protein kinase C lambda (PKC λ) in the development of obesity and glucose intolerance. *Adipocyte*. **1**: 203–214.
- Yi, C. X., O. Al-Massadi, E. Donelan, M. Lehti, J. Weber, C. Röss, C. Trivedi, T. D. Müller, S. C. Woods, and S. M. Hofmann. 2012. Exercise protects against high-fat diet-induced hypothalamic inflammation. *Physiol. Behav.* **106**: 485–490.
- García-Cáceres, C., E. Fuente-Martín, E. Burgos-Ramos, M. Granado, L. M. Frago, V. Barrios, T. Horvath, J. Argente, and J. A. Chowen. 2011. Differential acute and chronic effects of leptin on hypothalamic astrocyte morphology and synaptic protein levels. *Endocrinology*. **152**: 1809–1818.
- Lehti, M., E. Donelan, W. Abplanalp, O. Al-Massadi, K. M. Habegger, J. Weber, C. Röss, J. Mansfeld, S. Somvanshi, C. Trivedi, et al. 2013. High-density lipoprotein maintains skeletal muscle function by modulating cellular respiration in mice. *Circulation*. **128**: 2364–2371.
- Keuper, M., M. Jastroch, C-X. Yi, P. Fischer-Posovszky, M. Wabitsch, M. H. Tschöp, and S. M. Hofmann. 2014. Spare mitochondrial respiratory capacity permits human adipocytes to maintain ATP homeostasis under hypoglycemic conditions. *FASEB J.* **28**: 761–770.
- Brand, M. D. 2005. The efficiency and plasticity of mitochondrial energy transduction. *Biochem. Soc. Trans.* **33**: 897–904.
- Mrak, R. E., and W. S. T. Griffin. 2005. Glia and their cytokines in progression of neurodegeneration. *Neurobiol. Aging*. **26**: 349–354.
- Pekny, M., and M. Nilsson. 2005. Astrocyte activation and reactive gliosis. *Glia*. **50**: 427–434.
- Imai, Y., and S. Kohsaka. 2002. Intracellular signaling in M-CSF-induced microglia activation: role of Iba1. *Glia*. **40**: 164–174.
- Drake, C., H. Boutin, M. S. Jones, A. Denes, B. W. McColl, J. R. Selvarajah, S. Hulme, R. F. Georgiou, R. Hinz, A. Gerhard, et al. 2011. Brain inflammation is induced by co-morbidities and risk factors for stroke. *Brain Behav. Immun.* **25**: 1113–1122.
- Han, R., R. Lai, Q. Ding, Z. Wang, X. Luo, Y. Zhang, G. Cui, J. He, W. Liu, and Y. Chen. 2007. Apolipoprotein A-I stimulates

- AMP-activated protein kinase and improves glucose metabolism. *Diabetologia*. **50**: 1960–1968.
28. Vollenweider, P., A. von Eckardstein, and C. Widmann. 2015. HDLs, diabetes, and metabolic syndrome. *Handb. Exp. Pharmacol.* **224**: 405–421.
 29. Fuente-Martín, E., C. García-Cáceres, E. Morselli, D. J. Clegg, J. A. Chowen, B. Finan, R. D. Brinton, and M. H. Tschöp. 2013. Estrogen, astrocytes and the neuroendocrine control of metabolism. *Rev. Endocr. Metab. Disord.* **14**: 331–338.
 30. García-Cáceres, C., C-X. Yi, and M. H. Tschöp. 2013. Hypothalamic astrocytes in obesity. *Endocrinol. Metab. Clin. North Am.* **42**: 57–66.
 31. Kim, J. G., S. Suyama, M. Koch, S. Jin, P. Argente-Arizon, J. Argente, Z. W. Liu, M. R. Zimmer, J. K. Jeong, K. Szigeti-Buck, et al. 2014. Leptin signaling in astrocytes regulates hypothalamic neuronal circuits and feeding. *Nat. Neurosci.* **17**: 908–910.
 32. Horvath, T. L., B. Sarman, C. García-Cáceres, P. J. Enriori, P. Sotonyi, M. Shanabrough, E. Borok, J. Argente, J. A. Chowen, D. Perez-Tilve, et al. 2010. Synaptic input organization of the melanocortin system predicts diet-induced hypothalamic reactive gliosis and obesity. *Proc. Natl. Acad. Sci. USA*. **107**: 14875–14880.
 33. Stukas, S., J. Robert, M. Lee, I. Kulic, M. Carr, K. Tourigny, J. Fan, D. Namjoshi, K. Lemke, N. DeValle, et al. 2014. Intravenously injected human apolipoprotein A-I rapidly enters the central nervous system via the choroid plexus. *J. Am. Heart Assoc.* **3**: e001156.
 34. Song, Q., M. Huang, L. Yao, X. Wang, X. Gu, J. Chen, J. Huang, Q. Hu, T. Kang, Z. Rong, et al. 2014. Lipoprotein-based nanoparticles rescue the memory loss of mice with Alzheimer's disease by accelerating the clearance of amyloid-beta. *ACS Nano*. **8**: 2345–2359.
 35. Noe, N., L. Dillon, V. Lellek, F. Diaz, A. Hida, C. T. Moraes, and T. Wenz. 2013. Bezafibrate improves mitochondrial function in the CNS of a mouse model of mitochondrial encephalopathy. *Mitochondrion*. **13**: 417–426.
 36. Cavelier, C., P. M. Ohnsorg, L. Rohrer, and A. von Eckardstein. 2012. The β -chain of cell surface F(0)F(1) ATPase modulates apoA-I and HDL transcytosis through aortic endothelial cells. *Arterioscler. Thromb. Vasc. Biol.* **32**: 131–139.
 37. Cavelier, C., L. Rohrer, and A. von Eckardstein. 2006. ATP-binding cassette transporter A1 modulates apolipoprotein A-I transcytosis through aortic endothelial cells. *Circ. Res.* **99**: 1060–1066.
 38. Haddad-Tóvólli, R., N. R. V. Dragano, A. F. S. Ramalho, and L. A. Velloso. 2017. Development and function of the blood-brain barrier in the context of metabolic control. *Front. Neurosci.* **11**: 224.
 39. Vitali, C., S. A. Khetarpal, and D. J. Rader. 2017. HDL cholesterol metabolism and the risk of CHD: new insights from human genetics. *Curr. Cardiol. Rep.* **19**: 132.
 40. Favari, E., M. J. Thomas, and M. G. Sorci-Thomas. 2018. High-density lipoprotein functionality as a new pharmacological target on cardiovascular disease: unifying mechanism that explains high-density lipoprotein protection toward the progression of atherosclerosis. *J. Cardiovasc. Pharmacol.* **71**: 325–331.
 41. Pirillo, A., A. L. Catapano, and D. G. Norata. Biological consequences of dysfunctional HDL. *Curr. Med. Chem.* Epub ahead of print. May 29, 2018; doi:10.2174/0929867325666180530110543.
 42. Mayeux, R., and Y. Stern. 2012. Epidemiology of Alzheimer disease. *Cold Spring Harb. Perspect. Med.* **2**: a006239.